Structural and magnetic properties of $Fe_{3-x}V_xGe$ alloys

1990 J. Phys.: Condens. Matter 2 2997

(http://iopscience.iop.org/0953-8984/2/13/009)

J. Phys.: Condens. Matter 2 (1990) 2997–3006. Printed in the UK

Structural and magnetic properties of $Fe_{3-x}V_xGe$ alloys

A Beitollahi† and J G Booth
Department of Pure and Applied Physics, University of Salford, Salford M5 4WT, UK

Received 5 October 1989

Abstract. The crystallographic structure, atomic site occupancy and magnetic properties of a series of $Fe_{3-x}V_xGe$ alloys in the range $0 \leqslant x \leqslant 1.0$ have been determined. For $x \leqslant 0.4$ the HCP DO_{19}-type structure of the parent Fe_3Ge is retained but beyond this composition a tramsformation to the doubly ordered $L2_1$ Heusler structure occurs. Pulsed neutron diffraction measurements suggest that the V atoms enter one Fe site preferentially for the range $0.6 \leqslant x \leqslant 1.0$. The magnetisation, magnetic moment per Fe atom and Curie temperature all decrease with increasing x. In conjunction with magnetic susceptibility measurements carried out up to 900 K the results suggest that the $L2_1$ alloys have a largely itinerant character.

1. Introduction

The $Fe_{3-x}V_xGe$ system has a number of interesting features. Structurally, work on this and related systems has suggested that the progression from DO_{19} (or possibly $L1_2$ depending on heat treatment) through A2 (BCC) to A15 follows a decrease in the transition-metal electron concentration (Nakagawa and Kanematsu 1979). Furthermore, it is probable that the A2 alloys show additional ordering of the Heusler ($L2_1$) or DO_3 type. It is thus likely that magnetic atoms find themselves in differing environments in which they exhibit different magnetic moments. Measurements on isolated alloys from these systems show that the alloys have quite large magneto-optic Kerr rotations (Buschow *et al* 1983). Additionally, the A15 alloys near V_3Ge are superconducting but, as Fe is added to replace V, the suceptibility changes from Pauli paramagnetic to Curie–Weiss type indicative of increasing localised chacracter. We report here magnetic and structural studies of the system at the iron-rich end which have enabled the additional ordering in the A2 phase to be determined.

Earlier x-ray and magnetic studies of the system $Fe_{3-x}V_xGe$ have been carried out by Nakagawa and Kanematsu (1979) who reported that in the range beyond $x = 0.5$ the alloys showed a structural transition from that of the parent Fe_3Ge (HCP DO_{19}-type structure) to a BCC (A2) structure. Although their x-ray results did not indicate the presence of superlattice lines these workers suggested that the cubic alloys might be crystallographically ordered, possibly having the DO_3 or the $L2_1$ (Heusler) structure. In the present work, advantage has been taken of the irregular variation of neutron scattering length for neighbouring elements in the periodic table to determine the state of crystallographic order in this system using the Polaris instrument at the ISIS pulsed neutron facility at the Rutherford Appleton Laboratory. Probable site occupations have also been determined and the (>77 K) magnetisation measurements of Nakagawa and

† Present address: School of Materials, University of Leeds, Leeds LS2 9JT, UK.

0953-8984/90/132997 + 10 $03.50

Kanematsu (1979) have been extended down to 4.2 K. New susceptibility measurements for this range of x are reported.

2. Alloy fabrication and specimen preparation

The appropriate proportions of Spec-pure iron, vanadium and germanium metals were melted in an argon arc furnace, forming a series of alloy buttons of mass about 25 g which were powdered and annealed under vacuum in quartz capsules for 3 d at 900 °C to improve homogeneity. The capsules were then rapidly quenched into water. Subsequently x-ray and neutron diffraction data showed that all the members of the series were single phase except the compound with $x = 1.0$ for which a minute amount of second phase was detected. Each alloy was weighed before and after melting and the weight losses calculated. These were small (typically 0.5 wt% or less) and the nominal compositions were taken as accurate.

Magnetometer specimens were made from small pieces of material removed during the crushing process, which were then shaped into approximate ellipsoids for magnetisation measurements. These were annealed along with the powder in order to remove the initial strains due to pulverising and shaping.

3. Experimental techniques

3.1. Magnetisation measurements

Magnetic measurements were made over the range 4.2–900 K using a vibrating-sample magnetometer (Princeton Applied Research Corporation). Two specimens from each alloy were measured at room temperature to test the homogeneity of the materials. Low-temperature measurements on one of these were then obtained using a continuous-flow cryostat in which the sample temperature could be varied by adjustment of the temperature of helium gas flowing past the specimen (Oxford Instruments). The accuracy of measurement of the magnetisation was about 1% for the ferromagnetic samples. Measurements were made in fields up to 16 kG using a Varian 12 in magnet. Corrections for demagnetising fields were applied.

3.2. Pulsed neutron diffraction measurements

Room-temperature powder neutron diffraction measurements utilising a pulsed beam of unpolarised white neutrons were made at the Rutherford Appelton Laboratory, Chilton, using the Polaris diffractometer. The specimens were contained in vanadium cans during examination. Any magnetic contribution to the diffraction peaks at room temperature could be obtained by comparison of some well resolved peaks found at higher Q-values (greater than 10 Å^{-1}) with low-Q peaks for the same family of lines. The structure factors were obtained by measuring the areas under the Bragg peaks and assuming that

$$(\mathrm{d}\sigma/d\Omega)_\tau \sim (j\lambda^4/\sin^3\theta)|\mathrm{F}(\tau)|^2 \tag{1}$$

where $(\mathrm{d}\sigma/\mathrm{d}\Omega)_\tau$ is the cross section per Bragg reflection, and j and λ are the multiplicity factor and wavelength, respectively (Windsor 1981). $F(\tau)$ is the structure factor of a given reflection.

3.3. X-ray diffraction measurements

X-ray powder diffraction measurements at room temperature were performed using a Ievins–Straumanis camera and Fe Kα radiation of mean wavelength 1.9379 Å. Lattice parameters were determined by a Nelson–Riley extrapolation of the lattice parameters corresponding to each line.

4. Structure and atomic order

4.1. X-ray results

All the alloys were found to be single phase within the limits of experimental error except the sample with $x = 1.0$ for which a small amount of undetermined second phase was detected. The latter could not be identified as the anticipated A 15 β-W structure. The remaining x-ray diffraction patterns showed a structural transformation which occurred beyond $x = 0.4$. Two different structures were therefore distinguishable. One structure for the compositional range $0.6 \leqslant x \leqslant 1.00$ was attributed to a BCC structure at this stage, since no evidence of an ordered superlattice was found. Lattice parameters obtained from x-ray diffraction patterns using least-squares fits on Nelson–Riley plots did not appear sensitive to vanadium substitution in the case of the cubic structure, yielding a value for a_0 of 2.884 Å. The other structure for the compositional range $0 \leqslant x \leqslant 0.4$ was a HCP one of Ni_3Sn type with DO_{19} structure. Attempts to convert Fe_3Ge (and the other DO_{19} structures) to the $L1_2$ structure by prolonged heat treatment at 700 °C (Kanematsu 1963) were not successful.

4.2. Pulsed neutron diffraction results

Room-temperature diffraction patterns for the whole range of compositions studied are given in the multiplot version shown in figure 1. The two different sets of structural patterns can be clearly identified for the compositions with $0 \leqslant x \leqslant 0.4$ (figure 1(a)) and for $0.6 \leqslant x \leqslant 1.0$ (figure 1(b)). Some additional peaks relating to a second phase could be again found for the sample with $x = 1.0$. As can be seen in figure 1(b), for the compositions with $0.6 \leqslant x \leqslant 1.0$ the pulsed neutron diffraction patterns showed some additional order evidenced by the appearance of superlattice lines with h, k. l all odd and $(h + k + l)/2$ odd, as well as the fundamental reflections with $(h + k + l)/2$ even. These indices refer to the lattice introduced below and illustrated in figure 2 in which the cell edge of the BCC lattice mentioned above has been doubled.

4.2.1. Alloys in the range $0.6 \leqslant x \leqslant 1.0$. Analysis of the pulsed neutron diffraction data for these alloys showed that their structures could be discussed in terms of the unit cell illustrated in figure 2. The unit cell is composed of four interpenetrating FCC sublattices A, B, C and D with origins at the points (0, 0, 0), $(\frac{1}{4}, \frac{1}{4}, \frac{1}{4})$, $(\frac{1}{2}, \frac{1}{2}, \frac{1}{2})$ and $(\frac{3}{4}, \frac{3}{4}, \frac{3}{4})$. It can be shown as indicated above that Bragg reflections are produced by planes with Miller indices which are either all odd or all even, and three types of structure amplitude occur:

(i) h, k, l all odd

$$F^2(111) \sim (A - C)^2 + (B - D)^2 \tag{2a}$$

(ii) $(h + k + l)/2$ odd

$$F^2(200) \sim [(A + C) - (B + D)]^2 \tag{2b}$$

(iii) $(h + k + l)/2$ even

$$F^2(220) \sim [(A + C) + (B + D)]^2 \tag{2c}$$

Here A, B, C and D are the scattering lengths appropriate to each site. It is clear that

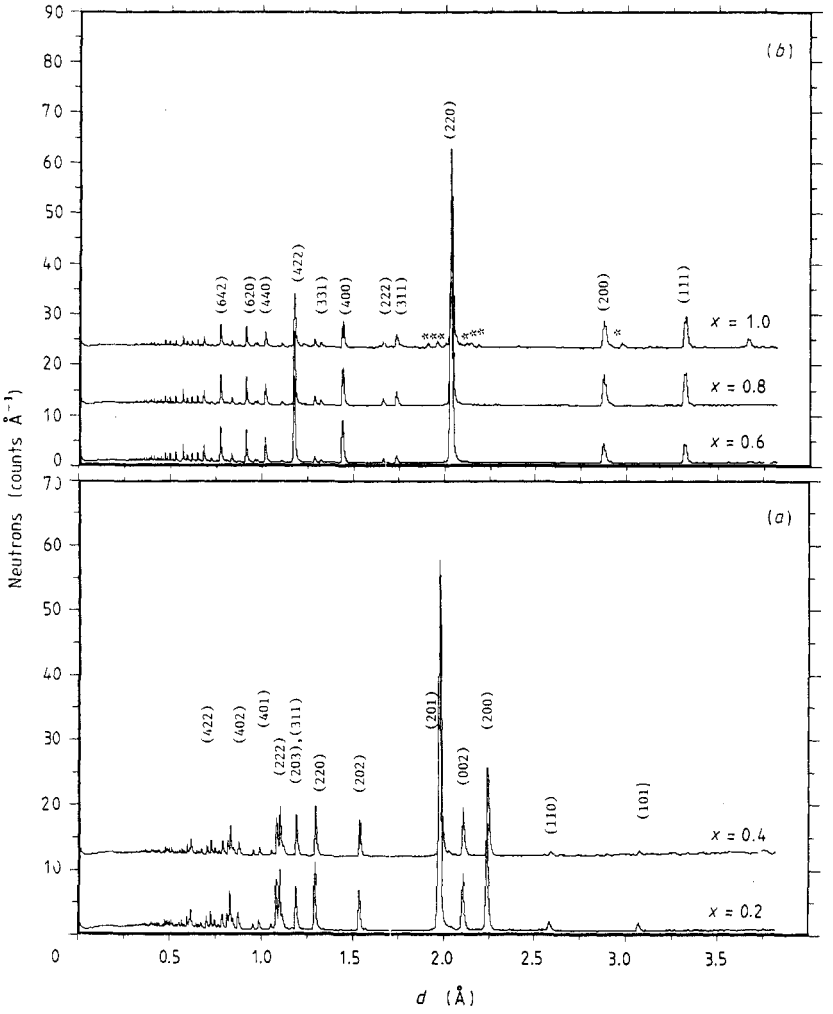

Figure 1. Room-temperature diffraction patterns for the $Fe_{3-x}V_xGe$ alloys: (*a*) results for alloys with $x = 0.2$ and 0.4, indicating a DO_{19} type structure; (*b*) results for $0.6 \leqslant x \leqslant 1.0$, indicating an $L2_1$ structure. The asterisks on the pattern for the alloy with $x = 1.0$ mark lines belonging to an additional unidentified phase.

the (220) line and its family are independent of atomic order and this line is used for normalising purposes. The parameters $\alpha = F^2(111)/F^2(220)$ and $\beta = F^2(200)/F^2(220)$ deduced from experimental intensities may then be compared with values calculated from appropriate models of site occupancy in order to determine the atomic arrangement of the unit cell. The x-ray atomic scattering factors of iron group transition metals are very close to each other and it is often difficult to deduce the type of order from x-ray data alone. For neutrons, however, the scattering lengths are not only largely different but sometimes also of opposite sign, e.g. in the present case V(−0.0385 fm), Fe(+0.954 fm) and Ge(+0.8186 fm) (Kostorz and Lovesey 1979). Thus neutron diffraction offers a sensitive technique for studying Fe–V and Ge–V disorder in these compounds. The x-ray and displacement densities were identical within experimental error so that the possibility of vacancy–vanadium disorder does not arise.

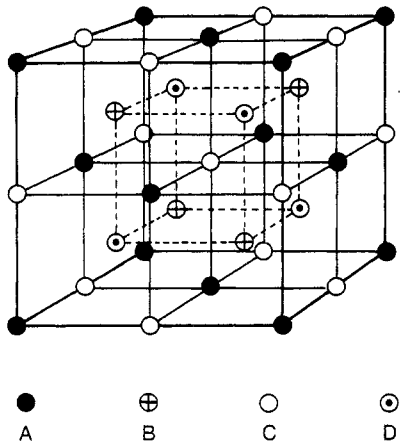

Figure 2. Unit cell formed by four interpenetrating FCC sublattices with origins at the points A (0, 0, 0), B ($\frac{1}{4}, \frac{1}{4}, \frac{1}{4}$), C ($\frac{1}{2}, \frac{1}{2}, \frac{1}{2}$) and D ($\frac{3}{4}, \frac{3}{4}, \frac{3}{4}$). For the $L2_1$ structure the A and C sites are occupied identically with different occupations of B and D sites, i.e. A ≡ C, B ≠ D. For the DO_3 structure, A ≡ B ≡ C ≡ D whereas, for the B2 structure, A ≡ C ≠ B ≡ D.

Table 1. Comparison of experimental and theoretical values of the ratios α and β for the alloys in the range $0.6 \leq x \leq 1.0$.

	Model (i) (DO_3)		Model (ii) ($L2_1C$)		Model (iii) ($L2_1A$)		Experimental	
Composition	α (10^{-2})	β (10^{-2})	α (10^{-2})	β (10^{-2})	α (10^{-2})	β (10^{-2})	α (10^{-2})	β (10^{-2})
$Fe_{2.4}V_{0.6}Ge$	0.004	0.004	0.19	2.3	2.22	5.61	2.45	5.5
$Fe_{2.2}V_{0.8}Ge$	0.20	0.20	0.22	5.20	5.20	10.36	5.43	9.79
$Fe_{2.0}V_{1.0}Ge$	0.53	0.53	0.25	10.1	10.1	17.61	9.1	18.40

Table 2. Site occupations assumed for model (i) (DO_3), model (ii) ($L2_1C$) and model (iii) ($L2_1A$).

		Site occupations in the following atomic sites			
Model		A	B	C	D
(i)	DO_3	Fe_{1-x} V_x	Fe_{1-x} V_x	Fe_{1-x} V_x	Ge
(ii)	$L2_1C$	Fe_{1-x} V_x	Fe	Fe_{1-x} V_x	Ge
(iii)	$L2_1A$	Fe	Fe_{1-x} V_x	Fe	Ge

The observed values of the quantities α and β were compared with those predicted by several theoretical models of the site occupancy and the results of the values obtained for some of the models attempted are shown in table 1. For model (i), the vanadium is assumed to occupy the A, B and C sites identically with Ge atoms alone occupying the D sites, i.e. a DO_3 structure (as shown in table 2). In model (ii) (referred to as $L2_1C$), the vanadium is considered to occupy the two sites A and C identically, with Fe and Ge on B and D sites, respectively. Model (iii) ($L2_1A$ structure), in which the two sites A

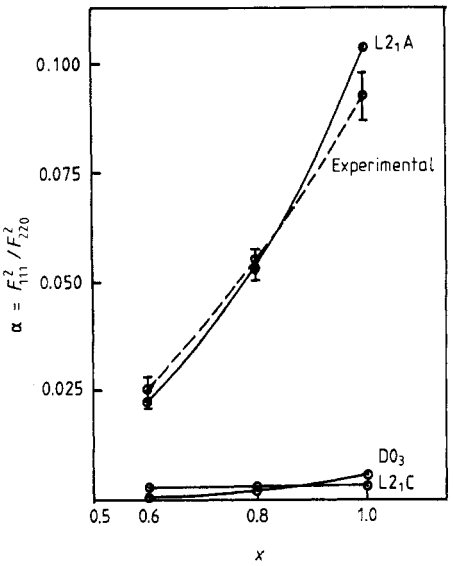

Figure 3. Variation in the parameter $\alpha = F^2(111)/F^2(220)$ versus x for the theoretical models indicated in table 1: ———, guide to the eye connecting the experimental results.

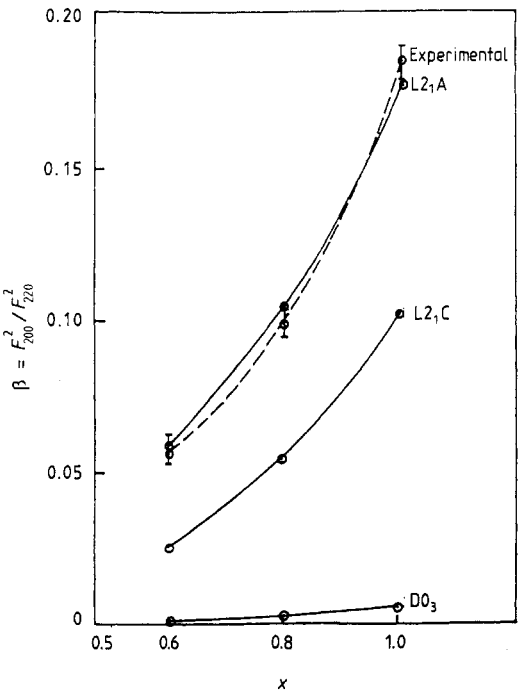

Figure 4. Variation in the parameter $\beta = F^2(200)/F^2(220)$ versus x for the theoretical models indicated in table 1: ———, guide to the eye connecting the experimental results.

and C are occupied solely by Fe atoms while site B is occupied by iron plus vanadium substituted for iron and site D germanium, is the only model which fits very closely to the observed values in the range $0.6 \leqslant x \leqslant 1.0$. Figures 3 and 4 show the curves of the variation in calculated and experimental values of the quantities α and β versus x at room temperature. The sensitivity to Fe–Ge disorder is lower than to Fe–V and Ge–V and it is, of course, possible to fit the observed intensities with a more complicated arrangement (involving, for example, equal occupation of the A and C sites by 0.96 Fe + 0.04 Ge together with a corresponding amount of Fe on the Ge D sites).

Table 3. The magnetic parameters for the system $Fe_{3-x}V_xGe$ for $0 \leq x \leq 1$.

Composition	Curie constant (10^{-3} K emu g^{-1} Oe^{-1})	q_c	q_s	q_c/q_s	Curie temperature (K)	θ_p (K)	$\sigma_{0.0}$ (emu g^{-1})	μ_{Fe} per Fe atom (μ_B)
				DO_{19} (Ni_3Sn) structures				
Fe_3Ge	21.45	5.50	6.43	0.86	634	655	149.5	2.14
$Fe_{2.6}V_{0.2}Ge$	21.32	5.46	5.74	0.95	559	572	134.0	2.05
$Fe_{2.6}V_{0.4}Ge$	20.2	5.28	4.89	1.08	476	498	114.6	1.88
				$L2_1$ structures				
$Fe_{2.4}V_{0.6}Ge$	11.8	3.85	2.40	1.60	459	510	56.6	1.00
$Fe_{2.2}V_{0.8}Ge$	8.62	3.16	1.25	2.52	255	366	29.5	0.56
$Fe_{2.0}V_{1.0}Ge$[a]	—	—	0.72	–	170	—	17.0	0.36

[a] Alloy with second phase.

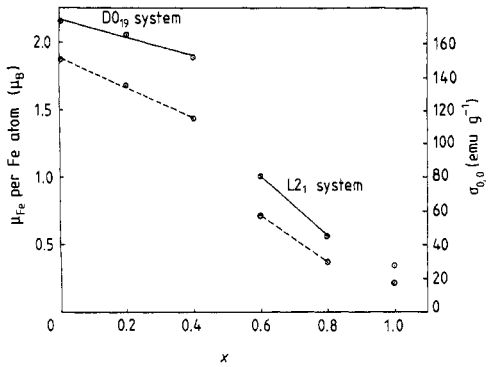

Figure 5. Variation in intrinsic magnetisation $\sigma_{0.0}$ (---) and magnetic moment) μ_{Fe} per Fe atom (———) versus x.

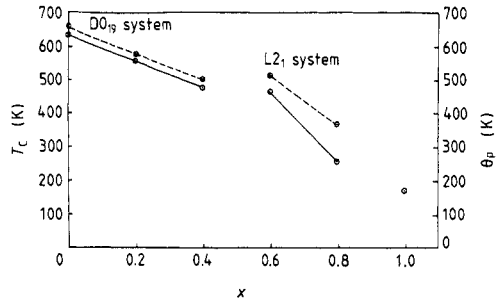

Figure 6. Variation in the ferromagnetic Curie temperature T_C (———) and the paramagnetic Curie temperature θ_p (---) versus x.

However, given the apparent antipathy of the Ge atoms for Fe sites, this structure seems unlikely and Occam's razor has been applied. Magnetic contributions to the diffracted lines were found negligible for the series of alloys with $L2_1A$ structure except for the case with $x = 0.6$ for which a very small magnetic contribution was measured by comparison of some well resolved peaks found at high Q-values with related low-Q peaks of the same family of lines. The magnetic form factor becomes negligible at higher Q (>10 Å^{-1}).

4.2.2. The composition range $0.0 < x < 0.4$. All the reflections expected from a HCP structure were found in the neutron diffraction patterns of the alloys with $x = 0.2$ and 0.4. These were similar to those appearing previously in the x-ray diffraction patterns, indicating a HCP structure of the (N_3Sn) DO_{19} type. The determination of a site occupancy of this structure was not attempted for these polycrystalline samples.

4.3. Magnetic measurements

Table 3 shows the various magnetic parameters obtained for the whole range of composition. The Curie temperatures T_C were determined by a modified Arrott (1957) plot method in which $\sigma^2_{H,T}$ and $H/\sigma_{H,T}$ isotherms are plotted and the isotherm which passes through the origin is taken to indicate T_C. Figure 5 shows the variation in intrinsic

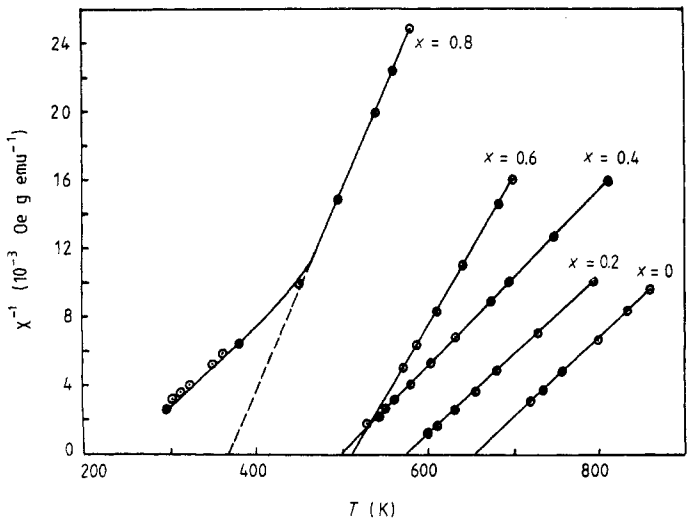

Figure 7. Inverse susceptibility $1/\chi$ versus temperature for the $Fe_{3-x}V_xGe$ alloys.

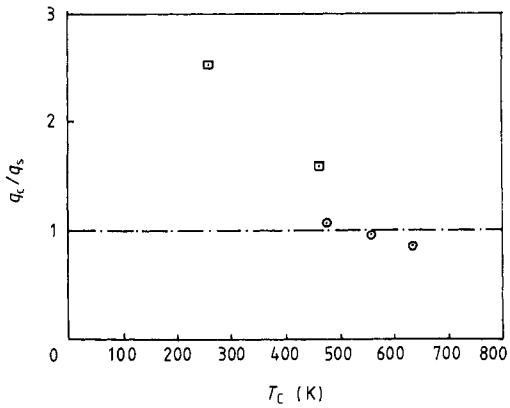

Figure 8. Rhodes–Wohlfarth (1963) plot of q_c/q_s versus Curie temperature for the $Fe_{3-x}V_xGe$ alloys: ⊡, cubic alloys; ⊙, hexagonal alloys.

magnetisation $\sigma_{0,T}$ and magnetic moment μ_{Fe} per iron atom, and figure 6 the Curie temperature T_C and paramagnetic Curie temperture θ_p versus the change in x. The variation in inverse susceptibility versus temperature is shown in figure 7 for the $0 \leqslant x \leqslant 0.8$ range. As these curves show, the slope of the lines corresponding to the compositions with $x = 0, 0.2$ and 0.4 are approximately equal, thus resulting in identical Curie constants within the limits of experimental error. Results of the variation in the quantity q_c/q_s (Rhodes and Wohlfarth 1963) where q_c is the paramagnetic moment determined using the relation $p_{eff}^2 = q_c\,(q_c + 2)$ are shown versus Curie temperature T_C in figure 8. Here p_{eff} is the effective paramagnetic moment per iron atom determined from high-temperature susceptibility measurements and q_s is the number of magnetic carriers per Fe atom deduced from low-temperature measurements of magnetisation.

5. Discussion and conclusions

As indicated above, the structural determinations have established that at low x the DO_{19} structure is appropriate and beyond $x = 0.6$ the presence of a (111) line indicates

the $L2_1$ structure. Since no attempt has been made to determine the site occupations in the former case, our discussion is limited to the $L2_1$ alloys in which it was found that the substituted V atoms enter one of three equivalent Fe sites (the B site). The A2 or DO_3 structures assigned to these alloys by Nakagawa and Kanematsu (1979) are therefore inappropriate. The A and C sites are magnetically and chemically distinct from the B site since they are surrounded by a first near-neighbour shell of four Fe and four Ge atoms whereas the B site has eight Fe near neighbours. The A and C sites have an environment which is progressively diluted in Fe as V is added whereas the Fe B site environment is unaffected. The situation is very similar to that existing when other transition metals are substituted for Fe in Fe_3Si (see, e.g., Booth 1988). A selective site occupation is found and neutron diffraction (Pickart *et al* 1975), NMR (Burch *et al* 1974) and Mössbauer results (Blaauw *et al* 1975) suggest that elements which are to the left of Fe in the periodic table (Ti, V, Cr and Mn) show a strong preference for B sites whereas Co and Ni exercise a preference for A and C sites. A calculation of the band structure of Fe_3Si and the local densities of states of the system with various impurities in the different sites (Garba and Jacobs 1986) has provided some theoretical justification for the site preferences found. The change in one-electron band energies when the impurity atom is moved from one site to another is calculated and the result for Mn and Co impurities gives a lower energy when the atoms are in the observed preferred sites. It seems probable that a similar explanation is appropriate for the Fe_3Ge alloys under discussion here.

Hines *et al* (1976) have discussed the magnetic behaviour of the Fe_3Si-based alloys and have given values of the rates of change of saturation moment $1/\sigma.\ d\sigma/dx$ and magnetic moment per atom $d\mu/dx$ for the various transition-metal impurities. For vanadium substitution in Fe_3Si they find values of $-3.94\mu_B$ and $-4.84\mu_B$ respectively. The results indicated in figure 5 suggest corresponding values of $-3.3\mu_B$ and $-2.5\mu_B$ for the Fe_3Ge system. These observed differences between the two systems suggest that the perturbation of the Fe (A and C) site moments depends on other factors in addition to the chemical nature of the substituted element. It should be mentioned that the values for the Fe_3Si system were obtained for very small dilutions ($x \leqslant 0.25$) and the indicated rates may diminish at higher values of x possibly as a result of changes in the second-nearest-neighbour interactions.

The inverse susceptibility curves shown in figure 7 indicate a constant slope for the DO_{19} alloys. Taken in conjunction with the decrease in saturation moment found, these results imply that the Rhodes–Wohlfarth ratio q_c/q_s is changing, but as indicated in figure 8 its value remains close to unity. It is not possible therefore to infer that a localised or itinerant model is appropriate in this case because for alloys with a high Curie temperature both models indicate a ratio of unity (Wohlfarth 1978). Moriya's (1979) intermediate model may provide an appropriate description of these alloys. In contrast, for the $L2_1$ alloys the Rhodes–Wohlfarth ratio is considerably larger, suggesting that the magnetism is best discussed in terms of an itinerant picture. Although the number of alloys that we have investigated is not sufficient to establish whether the changes in magnetisation and Curie temperature are linear with x, in conjunction with the results of Nakagawa and Kanematsu (1979), they indicate a linear variation. A linear dependence of x is expected on the basis of a band model and a quadratic variation if a localised model is appropriate. The result is a little surprising since in most Heusler compositions having the classical Heusler formula X_2YZ the Rhodes–Wohlfarth ratio is very close to unity and a number of indicators suggest that Heusler systems are often extremely well localised (Ziebeck *et al* 1983).

It was not possible in the time allocated to determine the site moments and it is planned to determine the variation in Fe I (A and C sites) and Fe II (B site) moments with x in the near future by low-temperature neutron diffraction.

Finally, the general observations of Nakagawa and Kanematsu on the stability of the $L2_1$ structure as the electron concentration is decreased suggest that the second phase in the alloy with $x = 1.0$ should have the A15 structure. It was not possible, however, to index the additional lines seen in the x-ray and neutron diffraction patterns of the alloy with $x = 1.0$ in terms of this structure.

Acknowledgments

The neutron scattering aspects of this research have been carried out under an agreement with the Neutron Beam Research Committee of the Science and Engineering Research Council. The authors are grateful to Dr J Mayers and the technical staff at the Rutherford Appleton Laboratory for their advice, expertise and support. The work was performed while A Beitollahi was working towards an MSc degree at the University of Salford (Beitollahi 1989).

References

Arrott A 1957 *Phys. Rev.* **108** 1394
Beitollahi 1989 Structural and magnetic properties of $Fe_{3-x}V_x$ Ge alloys *MSc Thesis* Salford University
Blaauw C, Mackay G R and Leiper W 1975 *Solid State Commun.* **18** 729
Booth J G 1988 Ferromagnetic transition metal intermetallic compounds *Ferromagnetic Materials* vol 4, ed E P Wohlfarth and K H J Buschow (Amsterdam: Elsevier) ch 3, pp 211 et seq
Burch T J, Litrenta T and Budnick J I 1974 *Phys. Rev. Lett.* **33** 421
Buschow K H J, van Engen P G and Jongebreur R 1983 *J. Magn. Magn. Mater.* **38** 1
Garba E J D and Jacobs R I 1986 *J. Phys. F: Met. Phys.* **16** 1485
Hines W A, Menotti A H, Budnick J I, Burch T J, Litrenta T, Niculescu V A and Raj K 1976 *Phys. Rev.* B **13** 4060
Kanematsu K 1963 *J. Phys. Soc. Japan* **18** 920
Kostorz G and Lovesey S W 1979 *Neutron Scattering—General Introduction in Treatise on Materials Science and Technology* vol 15, ed G Kostorz (New York: Academic) ch 1, p 1
Moriya T 1979 *J. Magn. Magn. Mater.* **14** 1
Nakagawa H and Kanematsu K 1979 *Japan. J. Appl. Phys.* **18** 1959
Pickart S J, Litrenta T, Burch T J and Budnick J I 1975 *Phys. Lett.* **53A** 321
Rhodes P and Wohlfarth E P 1963 *Proc. R. Soc.* A **273** 247
Windsor C G 1981 *Pulsed Neutron Scattering* (London: Taylor & Francis)
Wohlfarth E P 1978 *J. Magn. Magn. Mater.* 7 113
Ziebeck K R A, Brown P J, Deportes J, Givord D, Webster P J and Booth J G 1983 *Helv. Phys. Acta* **56** 117